

Identified high- p_T spectra in Cu+Cu collisions at $\sqrt{s_{NN}}=200$ GeV

B. I. Abelev,⁸ M. M. Aggarwal,³⁰ Z. Ahammed,⁴⁷ A. V. Alakhverdyants,¹⁷ B. D. Anderson,¹⁸ D. Arkhipkin,³
 G. S. Averichev,¹⁷ J. Balewski,²² L. S. Barnby,² S. Baumgart,⁵² D. R. Beavis,³ R. Bellwied,⁵⁰ F. Benedetto,²⁷
 M. J. Betancourt,²² R. R. Betts,⁸ A. Bhasin,¹⁶ A. K. Bhati,³⁰ H. Bichsel,⁴⁹ J. Bielcik,¹⁰ J. Bielcikova,¹¹ B. Biritz,⁶
 L. C. Bland,³ B. E. Bonner,³⁶ J. Bouchet,¹⁸ E. Braidot,²⁷ A. V. Brandin,²⁵ A. Bridgeman,¹ E. Bruna,⁵²
 S. Bueltmann,²⁹ I. Bunzarov,¹⁷ T. P. Burton,² X. Z. Cai,⁴⁰ H. Caines,⁵² M. Calderón de la Barca Sánchez,⁵
 O. Catu,⁵² D. Cebra,⁵ R. Cendejas,⁶ M. C. Cervantes,⁴² Z. Chajecski,²⁸ P. Chaloupka,¹¹ S. Chattopadhyay,⁴⁷
 H. F. Chen,³⁸ J. H. Chen,⁴⁰ J. Y. Chen,⁵¹ J. Cheng,⁴⁴ M. Cherney,⁹ A. Chikarian,⁵² K. E. Choi,³⁴ W. Christie,³
 P. Chung,¹¹ R. F. Clarke,⁴² M. J. M. Coddington,⁴² R. Corliss,²² J. G. Cramer,⁴⁹ H. J. Crawford,⁴
 D. Das,⁵ S. Dash,¹³ A. Davila Leyva,⁴³ L. C. De Silva,⁵⁰ R. R. Debbes,³ T. G. Dedovich,¹⁷ M. DePhillips,³
 A. A. Derevschikov,³² R. Derradi de Souza,⁷ L. Didenko,³ P. Djawotho,⁴² S. M. Dogra,¹⁶ X. Dong,²¹
 J. L. Drachenberg,⁴² J. E. Draper,⁵ J. C. Dunlop,³ M. R. Dutta Mazumdar,⁴⁷ L. G. Efimov,¹⁷ E. Elhalhuli,²
 M. Elnimr,⁵⁰ J. Engelage,⁴ G. Eppley,³⁶ B. Erazmus,⁴¹ M. Estienne,⁴¹ L. Eun,³¹ O. Evdokimov,⁸ P. Fachini,³
 R. Fatemi,¹⁹ J. Fedorisin,¹⁷ R. G. Fersch,¹⁹ P. Filip,¹⁷ E. Finch,⁵² V. Fine,³ Y. Fisyak,³ C. A. Gagliardi,⁴²
 D. R. Gangadharan,⁶ M. S. Ganti,⁴⁷ E. J. Garcia-Solis,⁸ A. Geromitsos,⁴¹ F. Geurts,³⁶ V. Ghazikhanian,⁶
 P. Ghosh,⁴⁷ Y. N. Gorbunov,⁹ A. Gordon,³ O. Grebenyuk,²¹ D. Grosnick,⁴⁶ B. Grube,³⁴ S. M. Guertin,⁶
 A. Gupta,¹⁶ N. Gupta,¹⁶ W. Guryn,³ B. Haag,⁵ T. J. Hallman,³ A. Hamed,⁴² L-X. Han,⁴⁰ J. W. Harris,⁵²
 J. P. Hays-Wehle,²² M. Heinz,⁵² S. Heppelmann,³¹ A. Hirsch,³³ E. Hjort,²¹ A. M. Hoffman,²² G. W. Hoffmann,⁴³
 D. J. Hofman,⁸ R. S. Hollis,⁸ H. Z. Huang,⁶ T. J. Humanic,²⁸ L. Huo,⁴² G. Igo,⁶ A. Iordanova,⁸ P. Jacobs,²¹
 W. W. Jacobs,¹⁵ P. Jakl,¹¹ C. Jena,¹³ F. Jin,⁴⁰ C. L. Jones,²² P. G. Jones,² J. Joseph,¹⁸ E. G. Judd,⁴ S. Kabana,⁴¹
 K. Kajimoto,⁴³ K. Kang,⁴⁴ J. Kapitan,¹¹ K. Kauder,⁸ D. Keane,¹⁸ A. Kechechyan,¹⁷ D. Kettler,⁴⁹ D. P. Kikola,²¹
 J. Kiryluk,²¹ A. Kisiel,⁴⁸ S. R. Klein,²¹ A. G. Knosp,⁵² A. Kocoloski,²² D. D. Koetke,⁴⁶ T. Kollegger,¹²
 J. Konzer,³³ M. Kopytine,¹⁸ I. Koralt,²⁹ W. Korsch,¹⁹ L. Kotchenda,²⁵ V. Kouchpil,¹¹ P. Kravtsov,²⁵ K. Krueger,¹
 M. Krus,¹⁰ L. Kumar,³⁰ P. Kurnadi,⁶ M. A. C. Lamont,³ J. M. Landgraf,³ S. LaPointe,⁵⁰ J. Lauret,³ A. Lebedev,³
 R. Lednicky,¹⁷ C-H. Lee,³⁴ J. H. Lee,³ W. Leight,²² M. J. LeVine,³ C. Li,³⁸ L. Li,⁴³ N. Li,⁵¹ W. Li,⁴⁰ X. Li,³³ X. Li,³⁹
 Y. Li,⁴⁴ Z. Li,⁵¹ G. Lin,⁵² S. J. Lindenbaum,²⁶ M. A. Lisa,²⁸ F. Liu,⁵¹ H. Liu,⁵ J. Liu,³⁶ T. Ljubicic,³ W. J. Llope,³⁶
 R. S. Longacre,³ W. A. Love,³ Y. Lu,³⁸ G. L. Ma,⁴⁰ Y. G. Ma,⁴⁰ D. P. Mahapatra,¹³ R. Majka,⁵² O. I. Mall,⁵
 L. K. Mangotra,¹⁶ R. Manweiler,⁴⁶ S. Margetis,¹⁸ C. Markert,⁴³ H. Masui,²¹ H. S. Matis,²¹ Yu. A. Matulenko,³²
 D. McDonald,³⁶ T. S. McShane,⁹ A. Meschanin,³² R. Milner,²² N. G. Minaev,³² S. Mioduszewski,⁴² A. Mischke,²⁷
 M. K. Mitrovski,¹² B. Mohanty,⁴⁷ M. M. Mondal,⁴⁷ D. A. Morozov,³² M. G. Munhoz,³⁷ B. K. Nandi,¹⁴
 C. Nattrass,⁵² T. K. Nayak,⁴⁷ J. M. Nelson,² P. K. Netrakanti,³³ M. J. Ng,⁴ L. V. Nogach,³² S. B. Nurushev,³²
 G. Odyniec,²¹ A. Ogawa,³ H. Okada,³ V. Okorokov,²⁵ D. Olson,²¹ M. Pachr,¹⁰ B. S. Page,¹⁵ S. K. Pal,⁴⁷
 Y. Pandit,¹⁸ Y. Panebratsev,¹⁷ T. Pawlak,⁴⁸ T. Peitzmann,²⁷ V. Perevoztchikov,³ C. Perkins,⁴ W. Peryt,⁴⁸
 S. C. Phatak,¹³ P. Pile,³ M. Planinic,⁵³ M. A. Ploskon,²¹ J. Pluta,⁴⁸ D. Plyku,²⁹ N. Poljak,⁵³ A. M. Poskanzer,²¹
 B. V. K. S. Potukuchi,¹⁶ C. B. Powell,²¹ D. Prindle,⁴⁹ C. Pruneau,⁵⁰ N. K. Pruthi,³⁰ P. R. Pujahari,¹⁴
 J. Putschke,⁵² R. Raniwala,³⁵ S. Raniwala,³⁵ R. L. Ray,⁴³ R. Redwine,²² R. Reed,⁵ J. M. Rehg,¹² H. G. Ritter,²¹
 J. B. Roberts,³⁶ O. V. Rogachevskiy,¹⁷ J. L. Romero,⁵ A. Rose,²¹ C. Roy,⁴¹ L. Ruan,³ M. J. Russcher,²⁷
 R. Sahoo,⁴¹ S. Sakai,⁶ I. Sakrejda,²¹ T. Sakuma,²² S. Salur,⁵ J. Sandweiss,⁵² E. Sangaline,⁵ J. Schambach,⁴³
 R. P. Scharenberg,³³ N. Schmitz,²³ T. R. Schuster,¹² J. Seele,²² J. Seger,⁹ I. Selyuzhenkov,¹⁵ P. Seyboth,²³
 E. Shahaliev,¹⁷ M. Shao,³⁸ M. Sharma,⁵⁰ S. S. Shi,⁵¹ E. P. Sichtermann,²¹ F. Simon,²³ R. N. Singaraju,⁴⁷
 M. J. Skoby,³³ N. Smirnov,⁵² P. Sorensen,³ J. Sowinski,¹⁵ H. M. Spinka,¹ B. Srivastava,³³ T. D. S. Stanislaus,⁴⁶
 D. Staszak,⁶ J. R. Stevens,¹⁵ R. Stock,¹² M. Strikhanov,²⁵ B. Stringfellow,³³ A. A. P. Suaide,³⁷ M. C. Suarez,⁸
 N. L. Subba,¹⁸ M. Sumner,¹¹ X. M. Sun,²¹ Y. Sun,³⁸ Z. Sun,²⁰ B. Surrus,²² T. J. M. Symons,²¹
 A. Szanto de Toledo,³⁷ J. Takahashi,⁷ A. H. Tang,³ Z. Tang,³⁸ L. H. Tarini,⁵⁰ T. Tarnowsky,²⁴ D. Thein,⁴³
 J. H. Thomas,²¹ J. Tian,⁴⁰ A. R. Timmins,⁵⁰ S. Timoshenko,²⁵ D. Tlusty,¹¹ M. Tokarev,¹⁷ T. A. Trainor,⁴⁹
 V. N. Tram,²¹ S. Trentalange,⁶ R. E. Tribble,⁴² O. D. Tsai,⁶ J. Ulery,³³ T. Ullrich,³ D. G. Underwood,¹
 G. Van Buren,³ G. van Nieuwenhuizen,²² J. A. Vanfossen, Jr.,¹⁸ R. Varma,¹⁴ G. M. S. Vasconcelos,⁷
 A. N. Vasiliev,³² F. Videbaek,³ Y. P. Vijoyi,⁴⁷ S. Vokal,¹⁷ S. A. Voloshin,⁵⁰ M. Wada,⁴³ M. Walker,²² F. Wang,³³
 G. Wang,⁶ H. Wang,²⁴ J. S. Wang,²⁰ Q. Wang,³³ X. Wang,⁴⁴ X. L. Wang,³⁸ Y. Wang,⁴⁴ G. Webb,¹⁹ J. C. Webb,⁴⁶
 G. D. Westfall,²⁴ C. Whitten Jr.,⁶ H. Wieman,²¹ E. Wingfield,⁴³ S. W. Wissink,¹⁵ R. Witt,⁴⁵ Y. Wu,⁵¹ W. Xie,³³
 N. Xu,²¹ Q. H. Xu,³⁹ W. Xu,⁶ Y. Xu,³⁸ Z. Xu,³ L. Xue,⁴⁰ Y. Yang,²⁰ P. Yepes,³⁶ K. Yip,³ I-K. Yoo,³⁴ Q. Yue,⁴⁴
 M. Zawisza,⁴⁸ H. Zbroszczyk,⁴⁸ W. Zhan,²⁰ S. Zhang,⁴⁰ W. M. Zhang,¹⁸ X. P. Zhang,²¹ Y. Zhang,²¹ Z. P. Zhang,³⁸
 J. Zhao,⁴⁰ C. Zhong,⁴⁰ J. Zhou,³⁶ W. Zhou,³⁹ X. Zhu,⁴⁴ Y. H. Zhu,⁴⁰ R. Zoukarneev,¹⁷ and Y. Zoukarneeva¹⁷

(STAR Collaboration)

- ¹Argonne National Laboratory, Argonne, Illinois 60439, USA
²University of Birmingham, Birmingham, United Kingdom
³Brookhaven National Laboratory, Upton, New York 11973, USA
⁴University of California, Berkeley, California 94720, USA
⁵University of California, Davis, California 95616, USA
⁶University of California, Los Angeles, California 90095, USA
⁷Universidade Estadual de Campinas, Sao Paulo, Brazil
⁸University of Illinois at Chicago, Chicago, Illinois 60607, USA
⁹Creighton University, Omaha, Nebraska 68178, USA
¹⁰Czech Technical University in Prague, FNSPE, Prague, 115 19, Czech Republic
¹¹Nuclear Physics Institute AS CR, 250 68 Řež/Prague, Czech Republic
¹²University of Frankfurt, Frankfurt, Germany
¹³Institute of Physics, Bhubaneswar 751005, India
¹⁴Indian Institute of Technology, Mumbai, India
¹⁵Indiana University, Bloomington, Indiana 47408, USA
¹⁶University of Jammu, Jammu 180001, India
¹⁷Joint Institute for Nuclear Research, Dubna, 141 980, Russia
¹⁸Kent State University, Kent, Ohio 44242, USA
¹⁹University of Kentucky, Lexington, Kentucky, 40506-0055, USA
²⁰Institute of Modern Physics, Lanzhou, China
²¹Lawrence Berkeley National Laboratory, Berkeley, California 94720, USA
²²Massachusetts Institute of Technology, Cambridge, MA 02139-4307, USA
²³Max-Planck-Institut für Physik, Munich, Germany
²⁴Michigan State University, East Lansing, Michigan 48824, USA
²⁵Moscow Engineering Physics Institute, Moscow Russia
²⁶City College of New York, New York City, New York 10031, USA
²⁷NIKHEF and Utrecht University, Amsterdam, The Netherlands
²⁸Ohio State University, Columbus, Ohio 43210, USA
²⁹Old Dominion University, Norfolk, VA, 23529, USA
³⁰Panjab University, Chandigarh 160014, India
³¹Pennsylvania State University, University Park, Pennsylvania 16802, USA
³²Institute of High Energy Physics, Protvino, Russia
³³Purdue University, West Lafayette, Indiana 47907, USA
³⁴Pusan National University, Pusan, Republic of Korea
³⁵University of Rajasthan, Jaipur 302004, India
³⁶Rice University, Houston, Texas 77251, USA
³⁷Universidade de Sao Paulo, Sao Paulo, Brazil
³⁸University of Science & Technology of China, Hefei 230026, China
³⁹Shandong University, Jinan, Shandong 250100, China
⁴⁰Shanghai Institute of Applied Physics, Shanghai 201800, China
⁴¹SUBATECH, Nantes, France
⁴²Texas A&M University, College Station, Texas 77843, USA
⁴³University of Texas, Austin, Texas 78712, USA
⁴⁴Tsinghua University, Beijing 100084, China
⁴⁵United States Naval Academy, Annapolis, MD 21402, USA
⁴⁶Valparaiso University, Valparaiso, Indiana 46383, USA
⁴⁷Variable Energy Cyclotron Centre, Kolkata 700064, India
⁴⁸Warsaw University of Technology, Warsaw, Poland
⁴⁹University of Washington, Seattle, Washington 98195, USA
⁵⁰Wayne State University, Detroit, Michigan 48201, USA
⁵¹Institute of Particle Physics, CCNU (HZNU), Wuhan 430079, China
⁵²Yale University, New Haven, Connecticut 06520, USA
⁵³University of Zagreb, Zagreb, HR-10002, Croatia

(Dated: November 3, 2018)

We report new results on identified (anti)proton and charged pion spectra at large transverse momenta ($3 < p_T < 10$ GeV/c) from Cu+Cu collisions at $\sqrt{s_{NN}} = 200$ GeV using the STAR detector at the Relativistic Heavy Ion Collider (RHIC). This study explores the system size dependence of two novel features observed at RHIC with heavy ions: the hadron suppression at high- p_T and the anomalous baryon to meson enhancement at intermediate transverse momenta. Both phenomena could be attributed to the creation of a new form of QCD matter. The results presented here bridge the system size gap between the available pp and Au+Au data, and allow the detailed exploration for the on-set of the novel features. Comparative analysis of all available 200 GeV data indicates that

the system size is a major factor determining both the magnitude of the hadron spectra suppression at large transverse momenta and the relative baryon to meson enhancement.

PACS numbers: 25.75.-q

Differential studies of identified particle production in nucleus-nucleus collisions provide an experimental means to probe the different stages of the collision evolution and explore the properties of the created medium. Spectral measurements at high transverse momenta are of special interest, for the following reasons. In elementary collisions, hard partonic scatterings are known to produce jets of particles originating from the fragmentation of a high- p_T quark or gluon. The spectral distributions of particles in transverse momentum from such interactions are measured experimentally and are reasonably well understood in terms of Next-to-Leading Order (NLO) pQCD calculations [1]. These hard scatterings occur in heavy-ion collisions as well, but their resulting distributions are found to be modified due to interactions with the medium and the resulting energy loss. Thus, understanding modifications to the high- p_T particle distributions is an important step towards understanding the partonic energy loss mechanisms within the medium [2].

To study the effects of parton-medium interaction on particle production in heavy-ion collisions we compare the production cross-sections measured in AA to the equivalent measurements in pp collisions. Following the expectation that the particle production in heavy-ion collisions at high- p_T is determined by the number of binary nucleon-nucleon inelastic collisions we define the nuclear modification factor, R_{AA} , as the ratio (Eq. (1)) of particle yields measured in AA to the cross-sections measured in pp collisions scaled by the corresponding number of independent nucleon-nucleon collisions N_{bin}^{AA} . We obtain N_{bin}^{AA} from a Monte Carlo Glauber model calculation [3]. For the unmodified particle production in AA collisions R_{AA} is exactly unity, whilst $R_{AA} < 1$ indicates *suppression* and $R_{AA} > 1$ *enhancement*.

$$R_{AA} = \frac{\sigma_{NN}^{\text{inel}}}{N_{\text{bin}}^{AA}} \frac{d^2 N_{AA}/dydp_T}{d^2 \sigma_{pp}/dydp_T}. \quad (1)$$

The R_{AA} measured in d +Au and peripheral Au+Au collisions exhibits an enhanced particle production which is believed to occur due to multiple nucleon scatterings within the colliding nuclei. This “initial” state effect is known as the Cronin effect [1, 4, 5]. Meanwhile, in central Au+Au collisions, R_{AA} at high- p_T indicates that the particle production is strongly suppressed (by about a factor of 5) [3, 6]. This “final” state effect has been attributed to the partonic energy loss in an opaque colored medium [7]. However, neither of the two effects is sufficiently understood and both require further experimental and theoretical study. The differential analysis presented here explores the system size effects on parton propagation through the medium to further evaluate the

mechanisms of parton/medium interactions.

To provide additional constraints and systematic understanding of the measurements in very light (d +Au) and heavy (Au+Au) collision systems we present the key studies at the intermediate (Cu+Cu) system at the same incident energy ($\sqrt{s_{NN}} = 200$ GeV), bridging the gap between the two extremes. These measurements may provide quantitative understanding of the partonic energy loss and its system size dependence. In addition, it is expected that the identified particle measurements provide information on color-charge effects within the mechanism of jet quenching. Although experimental discrimination between quark and gluon jet fragmentation on event-by-event basis is difficult, it can be addressed statistically by exclusive analysis of proton (or baryon) and pion (meson) production. We are utilizing the idea that the baryon to meson ratio is found higher in gluon jets compared to quark jets [8]. Identified proton and pion measurements from pp collisions concur with this picture [1, 9], as well as direct measurements of baryon and meson production in quark and gluon jets [10]. Thus, identified particle measurements at high- p_T can then be used to analyze gluon and quark propagation through the medium and to probe the color-charge differences of energy loss [2, 9, 11, 12].

Additionally, systematic studies of identified particle production in Cu+Cu can shed new light on the anomalous enhancement of baryons with respect to mesons observed at intermediate transverse momenta ($2 < p_T < 6$ GeV/ c) in Au+Au collisions. This enhancement is not consistent with the extrapolated values from the measurements in pp collisions and cannot be explained by cold nuclear matter effects. At present, the preferred baryon over meson production at intermediate p_T could be described by two very different considerations. The first model assumes coalescence and recombination, which demands a shift of baryon yields to higher momenta relative to meson yields [13]. The second model evokes an interplay of the flow effects in the radially expanding medium with the jet fragmentation [14].

In this paper identified (anti)proton and charged pion spectra are systematically explored with regard to the system size with the smaller Cu+Cu colliding system at $\sqrt{s_{NN}} = 200$ GeV. The centrality dependence of high- p_T hadron production and the p_T dependence of baryon to meson ratios in Cu+Cu data are compared to the Au+Au system as well as to pp collisions at the same energy. This allows gaining a greater understanding of *peripheral* collisions. The size of Cu nuclei is ideally suited to explore the turn-on of the high- p_T suppression bridging the gap between pp , d +Au and peripheral Au+Au data in terms of system size and nuclear matter.

The Cu+Cu data used in this analysis were recorded by the STAR experiment during Run 5 at RHIC. Here,

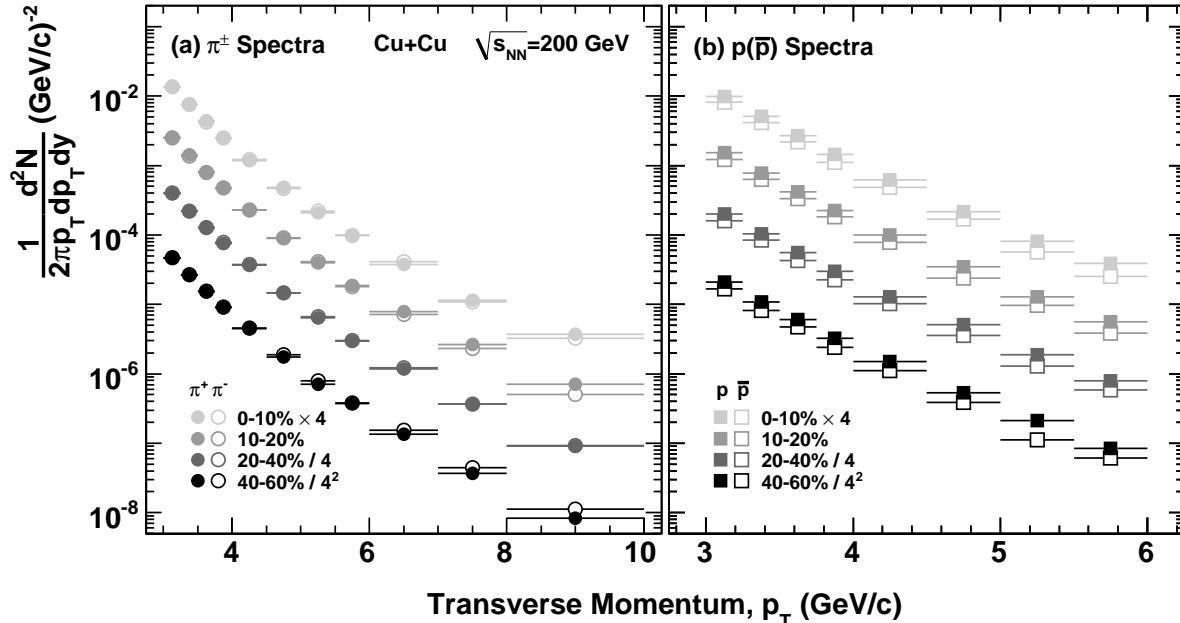


FIG. 1: Transverse momentum spectra of pions (a) and protons (b) produced in Cu+Cu collisions at $\sqrt{s_{NN}}=200$ GeV. Data are presented for four centrality classes: 0-10%, 10-20%, 20-40% and 40-60%. Closed and open symbols are used for particles and antiparticles, respectively. For clarity, data are separated by powers of four.

the minimum bias trigger was based on the combined signals from the Beam-Beam Counters at forward rapidity ($3.3 < |\eta| < 5.0$) and the Zero-Degree Calorimeters, located at ± 18 m from the nominal interaction point [15]. In total, 23 million events comprise this data set. Based on the charged track multiplicity recorded in the Time Projection Chamber (TPC) and Glauber MC model calculations, the data are divided into four centrality bins corresponding to 0-10%, 10-20%, 20-40% and 40-60% of fractional cross-section ($\sigma/\sigma_{\text{geom}}$) bins. In order to remove as many background tracks as possible, tracks which intercept the measured collision vertex within 1 cm (distance of closest approach) were retained with a minimum of 25 (out of 45) TPC trajectory points forming each track.

Within the STAR experiment, particle identification at low- p_T is attained by use of the ionization energy loss (dE/dx) in the TPC [16]. For low momentum particles, below 1 GeV/c, a clear mass separation is observed allowing the identification of π^\pm , K^\pm and (anti)protons. In the intermediate- p_T region ($1 < p_T < 3$ GeV/c) the TPC is no longer directly usable by itself, as all particles, independent of mass, are minimum ionizing. For the purpose of this paper we identify pions, kaons, protons and anti-protons at higher momenta ($p_T > 3$ GeV/c) on a statistical basis utilizing the relativistic rise of the ionization energy loss in the TPC. For a given slice in transverse momentum, a distinctly non-single-Gaussian shape

is observed, discussed in detail in [17], representing the normalized deviations from different energy loss trends of π , K and protons. The quantity used to express the energy loss is a normalized distribution, n_σ defined in Eq. (2), which accounts for the theoretical expectation (B_π , known as a Bichsel parameterization) and the resolution of the TPC for pions (σ_π).

$$n_\sigma = \log((dE/dx)/(B_\pi))/\sigma_\pi \quad (2)$$

The resultant distribution in each transverse momentum range is fit with a six-Gaussian function (one per particle-species/charge). The Gaussian widths are considered to be the same, independent of particle type, and single-Gaussian centroids are defined by the theoretical expectations constrained by the identified proton and pion measurements from topologically reconstructed weakly decaying particle yields [17]. Further details of the particle identification technique can be found in Refs. [1, 4].

Raw data yields are corrected for single-track inefficiencies evaluated via Monte-Carlo tracks embedded into real data events. We define single-track efficiency as the fraction of Monte Carlo tracks embedded into real Cu+Cu events that have been reconstructed. The efficiencies are derived for each different event multiplicity bin and particle species. For high- p_T tracks ($p_T > 2$ GeV/c) in 200 GeV Cu+Cu events, the efficiency is

found to be 85% on average, with a weak ($<10\%$) centrality and p_T dependence. In the analysis, pion and (anti)proton abundances are extracted from the n_σ distribution using the finely calibrated centroid positions. The derived kaon yields are then smoothed to reduce statistical fluctuations, using a Levy [1] fit. These assumed kaon spectra are then used for a final fit to determine the pion and proton yields. The systematic uncertainties from this procedure, on the spectra, are 2-10% for pions and 5-11% for protons, decreasing smoothly with p_T in the measured range. An analysis solving simultaneous equations to assumed pion, kaon and (anti)proton distributions (bin counting), derived results that are 5-10% (5-20%) higher for pions (protons). This difference is the dominant systematic uncertainty on particle spectra. An additional systematic error of 5% resultant from the uncertainty in the single-particle efficiency determination is added in quadrature. The total systematic error for pion spectra ranges from 9% (at 3 GeV/c) to 13% (at 10 GeV/c). For protons, the error ranges from 21% (at 3 GeV/c) to 23% (at 6 GeV/c). These uncertainties are similar to the earlier evaluation from Au+Au data analysis [9]. Systematic uncertainties from other possible sources such as the momentum resolution (studied by embedding) and the uncertainty in determination of the centroid position (within the particle identification procedure) are negligible. The corrected transverse momentum spectra for π^\pm and (anti)protons at $\sqrt{s_{NN}}=200$ GeV are shown in Fig. 1 (a) and (b) respectively. The reach in transverse momentum is limited only by the available statistics. Additional p_T reach for pion identification is due to a larger separation from the kaon peak ($\Delta\sigma_{\pi K} \sim 2\sigma$, $\Delta\sigma_{pK} \sim 1\sigma$).

Figure 2 shows π^-/π^+ and \bar{p}/p ratios in Cu+Cu data at $\sqrt{s_{NN}}=200$ GeV for the four centrality bins. The data show no systematic trends versus centrality within uncertainties, and a weak (if any) decreasing \bar{p}/p with transverse momentum (as observed in Au+Au collisions [9]). Thus, to improve the statistical uncertainties in the following discussion, data are averaged over particle charge.

The spectral data alone can convey only a limited message. To delve into properties of the resultant data, ratios are taken. The first such ratio is termed the nuclear modification factor (R_{AA}), defined in Eq. (1). We find that the pion spectra are suppressed in the most central (*head-on*) Cu+Cu data at $\sqrt{s_{NN}}=200$ GeV (Fig. 3). For the peripheral (*glancing*) collisions, a small enhancement is observed. To expose the features of the modifications of the hadron spectra in Cu+Cu and Au+Au collisions we study R_{AA} as a function of the amount of matter participating in the collisions. For both systems R_{AA} is evaluated within several fractional cross-section bins and as a function of the number of participating nucleons. Figure 3 (a) shows the results of this comparative analysis using the most central 0-12% (open squares) and mid-peripheral 40-60% (open circles) Au+Au data. For the most central events the suppression level is found to be different between the systems. The resultant spec-

tra from Au+Au collisions are more suppressed than in Cu+Cu data. According to the Glauber calculation the mid-central (20-40%) Cu+Cu collisions (closed circles) and mid-peripheral (40-80%) Au+Au data (open circles) have similar numbers of participating nucleons (see Appendix A for details). For this selection of centralities within the two systems we find that numerical values of R_{AA} agree within the uncertainties. This agreement suggests a correlation of the suppression with the initial volume of the collision system.

In Fig. 3 (b) we present the p_T averaged R_{AA} for pions ($5 < p_T < 8$ GeV/c) as a function of the number of participating nucleons calculated for both Cu+Cu and Au+Au collisions. The agreement between Au+Au (open circles) and Cu+Cu (closed circles) is striking and demonstrates that the nuclear modification factor for pions is a smooth function of the number of participating nucleons (independent of the collision system).

Similarly, we explore the systematics of baryon production in Cu+Cu and Au+Au systems by comparing the R_{AA} for protons and anti-protons. Figure 4 (a) shows the R_{AA} distributions averaged over p and \bar{p} for four centrality bins of Cu+Cu events. The data at hand does not differentiate if collision volume (N_{part}) or fractional cross-section effects are driving the high- p_T suppression for baryons due to the larger systematic uncertainties for (anti)proton measurements. Nevertheless, we observe that proton production in the peripheral Cu+Cu events is consistent with binary scaling expectations, and the suppression is setting in as one progresses from the peripheral to central events. An overall similar centrality dependence was observed between the Au+Au and Cu+Cu data at the same energy (see Fig. 4 (b)), albeit Cu+Cu integrated R_{AA} values seem lower than the respective Au+Au data points. We emphasize that the systematic errors are uncorrelated between the systems, and both measurements are similar within the experimental uncertainties.

The similarity between the different systems at the same number of participants is also evident in other aspects of the data at lower p_T [18]. The smooth dependence of the nuclear modification factor could be interpreted as a consequence of medium induced energy loss of partons traversing the hot and dense medium. For the smaller systems sizes, either peripheral Au+Au or Cu+Cu data, the path length traversed is smaller (on average) than for the larger system (central Au+Au). As observed in the data, a smaller energy loss is thus predicted [2].

Another dramatic effect observed in Au+Au data is the relative enhancement of protons to pions in the intermediate- p_T region as compared to pp and $e^+ + e^-$ collisions [9] as well as for other baryon to meson ratios [19]. This enhancement is found to be strongly dependent on the centrality of the collision, as illustrated in Fig. 5. The most peripheral A+A data is shown to exhibit little or no enhancement in this ratio, with respect to pp collisions at the same energy. A similar increasing

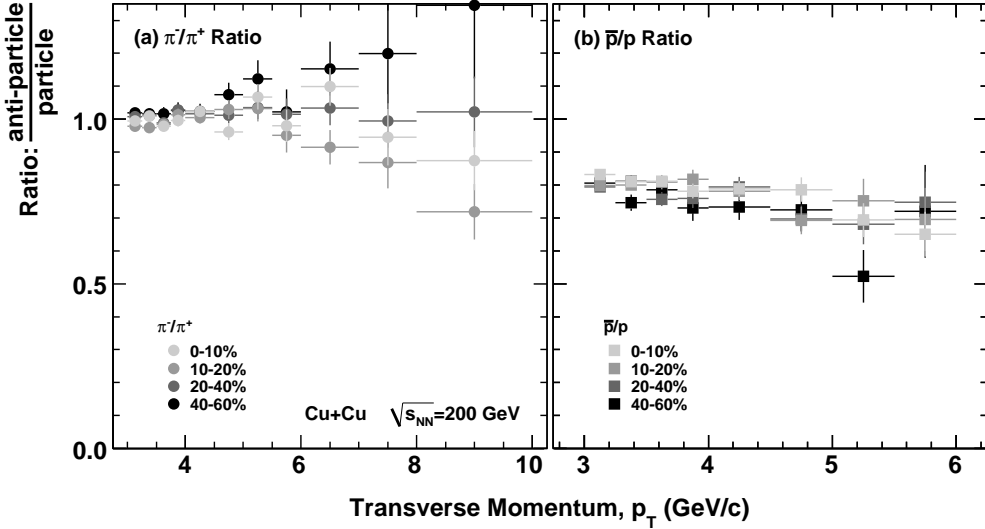


FIG. 2: Anti-particle to particle ratios, as a function of transverse momentum for pions (a) and protons (b). Data for the four centrality classes show little centrality dependence. Errors are statistical only.

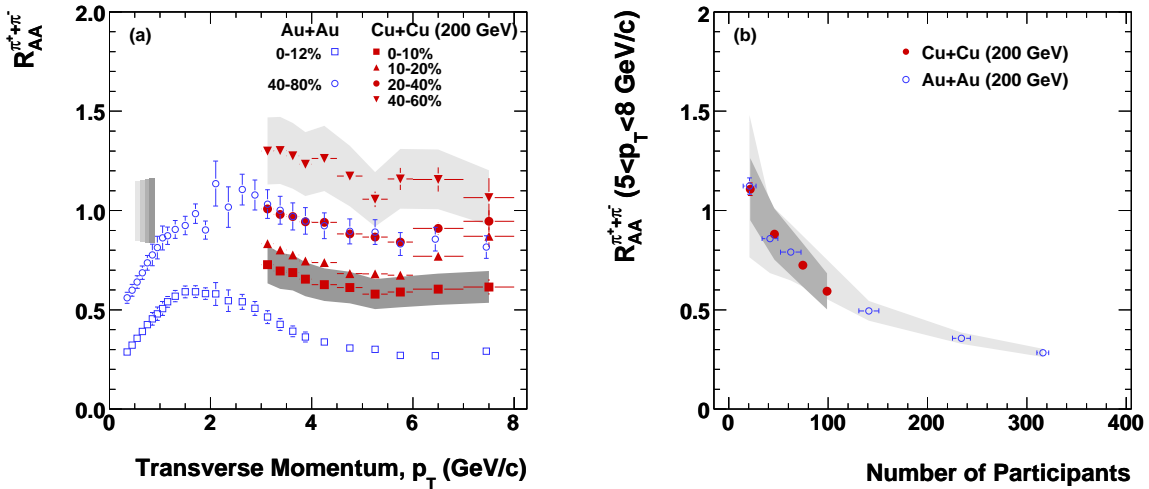


FIG. 3: (Color online) (a) Nuclear modification factor, R_{AA} , for charged pions ($\pi^+ + \pi^-$) in Cu+Cu (filled symbols) and Au+Au (open symbols) collisions at $\sqrt{s_{NN}}=200$ GeV. Error bands are shown for most peripheral and most central Cu+Cu data to represent evolution of the systematic uncertainties for this dataset. Error boxes at $R_{AA}=1$ represent Cu+Cu scale uncertainties due to the number of collisions and from pp spectra normalization. (b) Integrated pion R_{AA} over the range $5 < p_T < 8$ GeV/c versus N_{part} . The bands represent the systematic uncertainty on ratios. An additional scale error due to pp normalization ($\sim 14\%$) is not shown.

trend of favorable baryon production with centrality is observed in the Cu+Cu collision system. The peak of the enhancement is observed in the region $p_T \sim 2$ GeV/c in Au+Au, at a slightly lower transverse momentum than the range measured in this analysis. At higher transverse momenta the enhancement over pp collisions diminishes

to the level expected from vacuum fragmentation.

The baryon to meson ratio $(p+\bar{p})/(\pi^++\pi^-)$ in Cu+Cu and Au+Au collisions shows similar trends for an equivalent number of participating nucleons. To further quantify this observation Fig. 5 (b) shows the proton to pion ratio (for hadrons with $3 < p_T < 4$ GeV/c) measured in

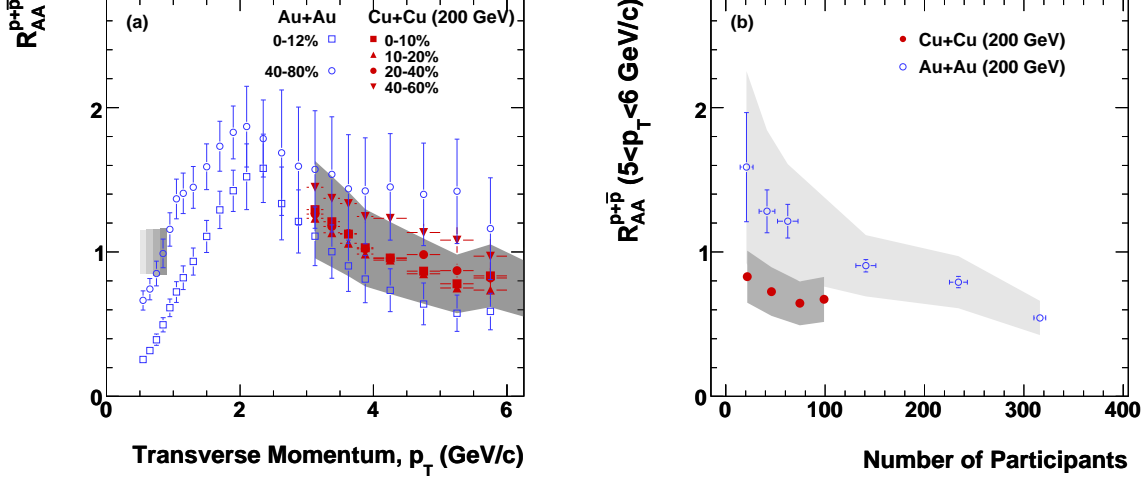


FIG. 4: (Color online) (a) Nuclear modification factor, R_{AA} , for protons and anti-protons ($p + \bar{p}$) in Cu+Cu (filled symbols) and Au+Au (open symbols) collisions at $\sqrt{s_{NN}}=200$ GeV. Error band is shown for most central Cu+Cu data to represent characteristic systematic uncertainties for Cu+Cu data. Error boxes at $R_{AA}=1$ represent Cu+Cu scale uncertainties due to the number of collisions and from pp spectra normalization. (b) Integrated (anti)proton R_{AA} over the range $5 < p_T < 6$ GeV/c versus N_{part} . The bands represent the systematic uncertainty on ratios. An additional scale error due to pp normalization (about 14%) is not shown.

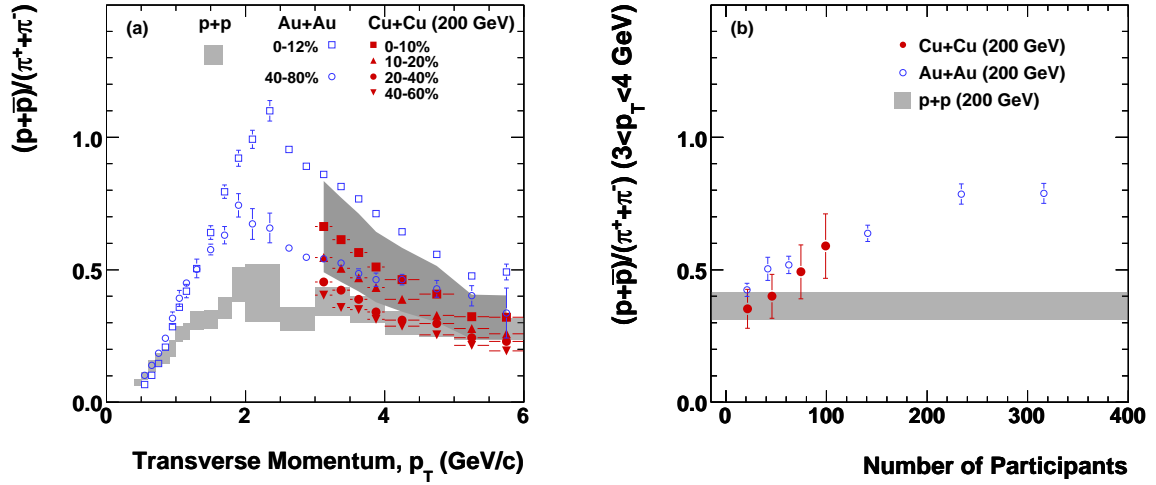


FIG. 5: (Color online) (a) Ratio of protons and anti-protons to charged pions, versus transverse momentum, for Cu+Cu collisions at $\sqrt{s_{NN}}=200$ GeV. For clarity, only one systematic error band is shown for Cu+Cu data (most central events), uncertainties on data in other centrality bins are similar in magnitude. Systematic errors for Au+Au data are not shown, for details see [9]. (b) Average $(p + \bar{p})/(\pi^+ + \pi^-)$ ratio for $3 < p_T < 4$ GeV/c is shown as function of centrality (N_{part}) for Cu+Cu and Au+Au data. Error band represents the pp measurement with uncertainty.

Cu+Cu and Au+Au collisions as a function of N_{part} . We find that this ratio is also sensitive to the initial volume of the collision system and exhibits the same quantitative N_{part} dependence irrespective of the collision system.

As discussed earlier, it is found that in the kinematic range of our measurements baryons are produced pre-

dominantly from gluon fragmentation [20]. It is thus expected that an increase in the baryon to meson ratio in the intermediate- to high- p_T range would be related to gluon sources. To explain the presented data one could consider, for example, that a gluon jet could be more easily propagated through the medium than a

quark jet, leading to an increase in the number of protons in the intermediate- p_T region. This, however contradicts theoretical predictions where an opposite effect was expected [2]. Alternatively, more gluon jets could be initially produced, or *induced* (for example, in the radiative energy loss scenario), for the more central data. The latter appears to be the more plausible, as the highest p_T data exhibits little or no enhancement over the pp data, indicating a similar energy loss for gluons and quarks (see Fig. 5). Alternative approaches to explain the phenomenon observed in the data, have also been developed. For example, the recombination/fragmentation picture of thermal/shower partons has had success at describing this in Au+Au data [13]. Further information on the relative energy loss of quark and gluon jets can be extracted from the data by comparing the nuclear modification factors of proton and pion data (Figs. 3 and 4). At high- p_T (above 5 GeV/c), however, the two suppression factors are found to be the same within the systematic uncertainties, suggesting a similar energy loss of quark and gluon jets in Cu+Cu collisions.

In conclusion, new results on high- p_T identified pion and proton spectra are presented for several centrality

bins in Cu+Cu collisions at $\sqrt{s_{NN}}=200$ GeV. The data are found to exhibit similar systematic trends over a wide range of transverse momenta as Au+Au collisions at the same energy with a similar number of participants. The suppression pattern observed versus the number of participants in Au+Au data is followed by the Cu+Cu data to a large degree. The participant coverage in these Cu+Cu collisions is in a region where the suppression effects are turning on. A detailed study of the proton to pion ratio reveals similar systematic dependencies to that found in Au+Au data. Specifically, the increase in proton yield at intermediate transverse momenta persists for the much smaller Cu+Cu system.

Further studies have shown similar suppression of protons and pions at high- p_T . Within the context of the connection between the detected pions and protons and quark and gluon jets suggested in the introduction, these results indicate similar partonic energy loss for both gluons and quarks. The amount of energy loss suffered by the partons is found to be N_{part} dependent. Within the experimental uncertainties, the suppression for different collision species is found to be invariant for the same number of participants.

-
- [1] J. Adams *et al.* *Phys. Lett.* **B637** (2006) 161.
 - [2] I. Vitev *Phys. Lett.* **B639** (2006) 38.
 - [3] J. Adams *et al.* *Phys. Rev. Lett.* **91** (2003) 172302.
 - [4] J. Adams *et al.* *Phys. Lett.* **B616** (2005) 8.
 - [5] D. Antreasyan *et al.* *Phys. Rev.* **D19** (1979) 764.
 - [6] C. Adler *et al.* *Phys. Rev. Lett.* **90** (2003) 082302.
 - [7] J. Adams *et al.* *Phys. Rev. Lett.* **91** (2003) 072304.
 - [8] K. Konishi *et al.* *Phys. Lett.* **B78** (1978) 243.
 - [9] B. I. Abelev *et al.* *Phys. Rev. Lett.* **97** (2006) 152301.
 - [10] P. Abreu *et al.* *Eur. Phys. J.* **C17** (2000) 207.
 - [11] B. Mohanty *J. Phys. G* **34** (2007) S793.
 - [12] B. I. Abelev *et al.* *Phys. Lett.* **B655** (2007) 104.
 - [13] R. C. Hwa and C. B. Yang *Phys. Rev. C* **70** (2004) 024905.
 - [14] C. M. Hung and E. Shuryak *Phys. Rev. C* **57** (1998) 1891.
 - [15] C. Adler *et al.* *Nucl. Instr. Meth.* **A461** (2001) 337.
 - [16] M. Anderson *et al.* *Nucl. Instrum. Meth.* **A499** (2003) 659.
 - [17] Y. Xu *et al.* arXiv:nucl-ex/0807.4303.
 - [18] A. Iordanova *et al.* *J. Phys. G* **35** (2008) 044008.
 - [19] B. I. Abelev *et al.* arXiv:nucl-ex/0601042 *submitted to Phys. Rev. C.*
 - [20] S. Albino *et al.* *Nucl. Phys.* **B725** (2005) 181.

Acknowledgments

We thank the RHIC Operations Group and RCF at BNL, the NERSC Center at LBNL and the Open Science Grid consortium for providing resources and support. This work was supported in part by the Offices of NP and HEP within the U.S. DOE Office of Science, the U.S. NSF, the Sloan Foundation, the DFG clus-

ter of excellence ‘Origin and Structure of the Universe’, CNRS/IN2P3, STFC and EPSRC of the United Kingdom, FAPESP CNPq of Brazil, Ministry of Ed. and Sci. of the Russian Federation, NNSFC, CAS, MoST, and MoE of China, GA and MSMT of the Czech Republic, FOM and NOW of the Netherlands, DAE, DST, and CSIR of India, Polish Ministry of Sci. and Higher Ed., Korea Research Foundation, Ministry of Sci., Ed. and Sports of the Rep. Of Croatia, Russian Ministry of Sci. and Tech, and RosAtom of Russia.

**APPENDIX A: MONTE CARLO GLAUBER
MODEL RESULTS FOR THE CENTRALITY
BINS USED IN THE PAPER**

TABLE I: Number of participants N_{part} and number of binary collisions N_{bin} from the Monte Carlo Glauber model calculations for different centrality bins of minimum bias Cu+Cu collisions at 200 GeV.

| Centrality bin | N_{part} | N_{bin} |
|----------------|----------------------|-------------------------|
| 0-10% | $99.0^{+1.5}_{-1.2}$ | $188.8^{+15.4}_{-13.4}$ |
| 10-20% | $74.6^{+1.3}_{-1.0}$ | $123.6^{+9.4}_{-8.3}$ |
| 20-40% | $45.9^{+0.8}_{-0.6}$ | $62.9^{+4.2}_{-3.7}$ |
| 40-60% | $21.5^{+0.5}_{-0.3}$ | $22.7^{+1.2}_{-1.1}$ |

TABLE II: Number of participants N_{part} and number of binary collisions N_{bin} from the Monte Carlo Glauber model calculations for different centrality bins of minimum bias Au+Au collisions at 200 GeV.

| Centrality bin | N_{part} | N_{bin} |
|----------------|-----------------------|-------------------------|
| 10-20% | $234.6^{+8.3}_{-9.3}$ | $591.3^{+51.9}_{-59.9}$ |
| 20-40% | $141.4^{+9.9}_{-9.5}$ | $294.2^{+40.6}_{-39.9}$ |
| 40-60% | $62.4^{+8.3}_{-10.4}$ | $93.6^{+17.5}_{-23.4}$ |
| 60-80% | $20.9^{+5.1}_{-6.5}$ | $21.2^{+6.6}_{-7.9}$ |
| 40-80% | $41.5^{+6.9}_{-6.6}$ | $57.1^{+13.7}_{-13.3}$ |

TABLE III: Number of participants N_{part} and number of binary collisions N_{bin} from the Monte Carlo Glauber model calculations for 200 GeV central triggered Au+Au collisions.

| Centrality bin | N_{part} | N_{bin} |
|----------------|-----------------------|-------------------------|
| 0-12% | $315.7^{+5.6}_{-4.5}$ | $900.3^{+71.4}_{-63.7}$ |